

## Design of the Structural Behaviour of a Nozzle Charged by Primary Loads and Cyclic Thermal Shocks

F. Corsi, G.M. Giannuzzi, P. Di Giamberardino

*ENEA C.R.E. Casaccia, VEL/MEP/TERMO, S.P. Anguillarese 301, C.P. 2400, I-00100 Roma, Italy*

B. Taddia

*ENEA, Dipartimento Reattori Veloci, Via dell'Arcoveggio 56/23, I-40129 Bologna, Italy*

### Abstract

The paper presents the scheme followed for the design verification of the structural behaviour of a nozzle charged by primary three-dimensional loads and cyclic thermal shocks. The standard limits defined in ASME N47 appendix are used as rules both for an elastic analysis and for a detailed inelastic study.

The simplified way of dealing the problem by an axisymmetric computer program is pointed out. Both the elastic and inelastic analysis were carried out with the general purpose CASTEM system developed at CEA in Saclay.

The main conclusions of the application of the different existing rules are presented.

### 1. Introduction

Fig.1 shows the IPM/2 section test; it is formed by two big tanks SE20 and SE21 ( $V=12$  mC), a control-valve WP210 and an helicoidal connection pipeline EL26 ( $L=28$  m,  $\phi_e=324$  mm and  $S=4$  mm). During the pre-shock phase different temperatures are obtained along the pipeline length by means of electric warming cables. The temperature varies from  $550^\circ\text{C}$  at the SE20 tank to about  $400^\circ\text{C}$  at SE21. When the valve is opened about 2000 litres of sodium flow in 10 sec inside the latter tank realizing a cold shock.

A conical nozzle connects the helicoidal pipeline to the SE20 tank. The nozzle is provided by an inner thermal baffle so to reduce the stress level on this critical structure, that is subjected to the same severe cold thermal cycling shocks that charge the PEC mechanism. The detailed drawing of the nozzle thermal baffle component is shown in Fig.2.

A refined experimental-theoretical study was conducted to verify the structural behaviour of this component according the existing standards rules for high temperature operating service.

### 2. Experimental study

To verify the operative conditions a series of ten experimental cycles was performed. The nozzle was instrumented on the outer surface with thermocouples and resistive strain gages in the axial and circumferencial directions (Fig.2). A large part of the instrumentation was concentrated around the critical welded zones.

The experimental recordings gave the necessary elements for the theoretical comparison.

### 3. Design verification scheme

The design verification was conducted both on elastic analysis data and refined inelastic study. All the used computer codes are part of the finite element CASTEM system develo-

ped at CEA in Saclay. The scheme used for the discretization of the structure is shown in figg. 3 and 4. The applied standard rules are the ASME N47 codes.

It is to point out that the followed procedure can be accepted as general way to verify the structural behaviour of LMFBR components subjected to low primary loads caused by the connected layout and to severe secondary cycling thermal shocks.

The stress-strain analysis of the component was conducted in the following detailed way:

- a) value definition of the primary charges transmitted to the component by the layout of which is part (fig.5 and 6). The first step, performed in elastic field, allowed to find the values of the various loads  $M_{fx}$ ,  $M_{fy}$  (Bending moments),  $T_x$ ,  $T_y$  (Shear forces),  $M_z$  (Twisting moment),  $N_z$  (Traction charge) acting on the initial reference of the structure (Section A of fig.2)
- b) Fourier series analysis on the base of the first armonic of the non-axialsymmetric loads to have the elastic stress field caused by abovesaid load state on the nozzle (fig.7).
- c) marking out on the most stressed zone (B of fig.2) and of the critical symmetric plane (fig.8.).
- d) definition of the secondary stress field in the thermal transient.

It is to point out that generally for LMFBR components the primary loads are very low respect to the secondary stress. This allows elastic analysis for the piping effects and requires detailed non-linear thermal-structural studies.

For example, in this case on the base of a fluid-dynamic analysis that defined the sodium flow-rate between the nozzle and the thermal baffle a non linear thermal transient study was carried out.

The theoretical-experimental comparison of the trend of temperature in time at different heights(fig.9 ) showed a very good identity and gave proof of the good definition of the thermal charge input, of primary importance for the successive structural study.

Clearly in elastic study for the allowed effects superposition it is possible to find single load actions and to follow simply all the rules defined in ASME N47 appendix. So in a first step a thermo-structural analysis was performed that gave the secondary stress state caused by the thermal shocks. The obtained results were in a good agreement with the relevant experimental curves (fig.10) related to the hoop and axial strains versus time.

The standard rules showed a respect of the component structural behaviour for Test 3 of N47 appendix and a number of load cycles limited to about 100 for creep-fatigue damage in the most stressed section B. The too restricted evaluated life showed as necessary an inelastic study.

So if one is forced to go to an inelastic analysis, as for this case, it is necessary to follow a semplified but detailed scheme for the respect of the inelastic limits. The problem is reduced to define the axialsymmetric loads "equivalent" to the complexive action of the different primary charges.

For this case an axialsymmetric traction charge acting on section A (fig. 2) gave a similar stress state (fig.11). This allowed to pass to an inelastic detailed analysis for three load cycles (fig.12).

#### 4. Conclusions

Verification of the ASME rules were interily satisfied /6/. It appeared necessary for this case an inelastic study, in fact the allowed creep-fatigue cycles showed a factor of about 50 passing from elasting routes to the inelastic ones.

The work seems to show from one side a good reliability of the available analitical tools and from the other a necessary effort for a deeper study in the creep-fatigue damage modes. On the same time further instrumentation (thermocouples and 12 resistive strain gages) was put around the most stressed zone (section B) to have more experimental details for this critical welded section.

REFERENCES

- /1/ O.C. ZIENKIEWICZ "The Finite Element Method", Mc Graw-Hill.
- /2/ F. CESARI "Il metodo degli Elementi Finiti nei problemi termostrutturali", Pitagora editrice, Bologna.
- /3/ J.C. MASSON, "Castem", Compagnie Internationale de Services en Informatique, Novembre 1979 Parigi.
- /4/ A. HOFFMANN, F. JEANPIERRE, M. LIVOLANT, "Aperçus théorique sur les programmes. Elements Dynamique. Non linéarités géométriques. Flamlage. Plasticité". Note CEA -N -1934 - CEN Saclay.
- /5/ F. CORSI, "Verifica dell'affidabilità del codice ad elementi finiti INCA in un'analisi ciclica elasto-plastica creep", RT/ING (80) 7, CNEN.
- /6/ ASME; CODE CASE N47-12.

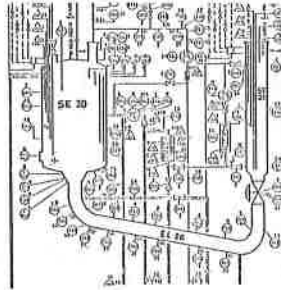


Fig.1 - IPM/2 sodium loop

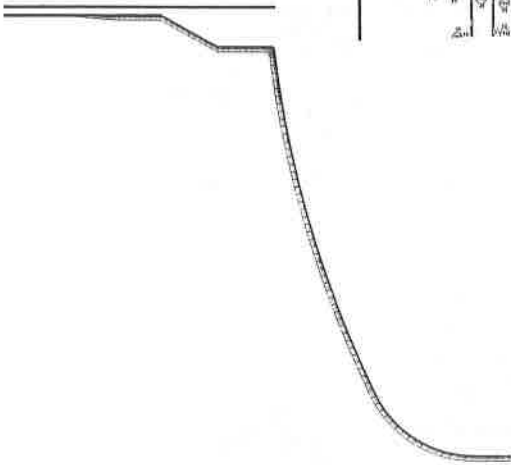


Fig.2 - Thermocouples and strain-gages location on the nozzle

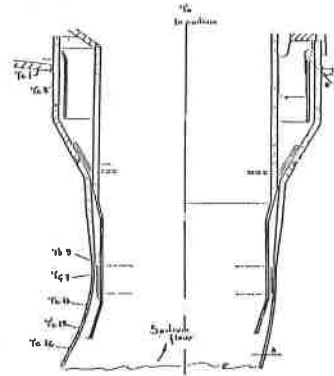


Fig.3 - Discretization for thermal analysis

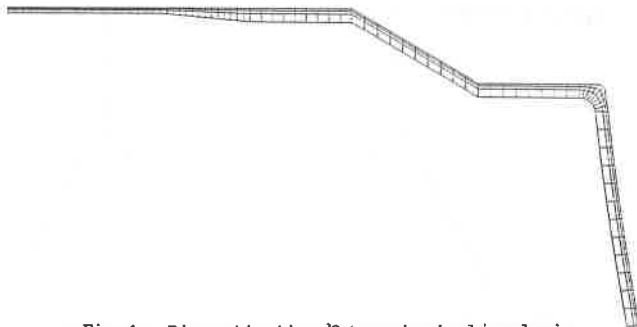


Fig.4 - Discretization for mechanical analysis

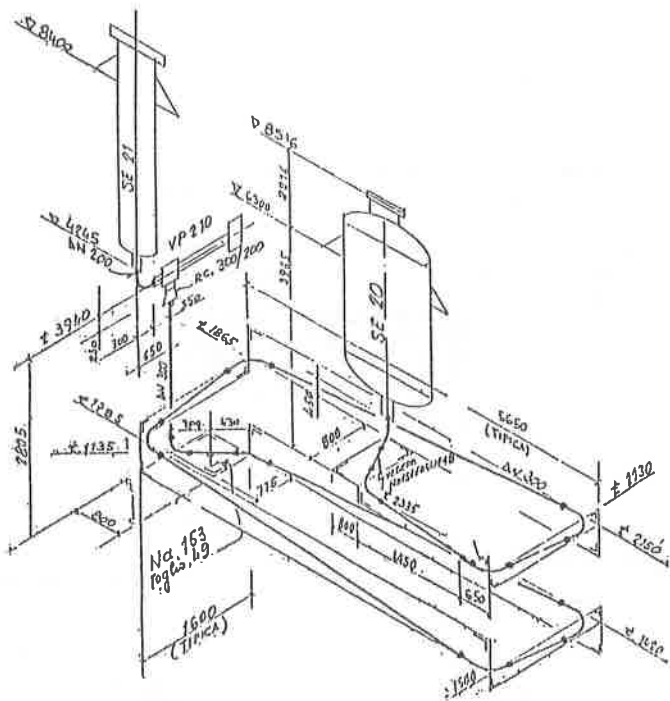


Fig.5 - Threedimensional drawing of IPM/2 sodium loop

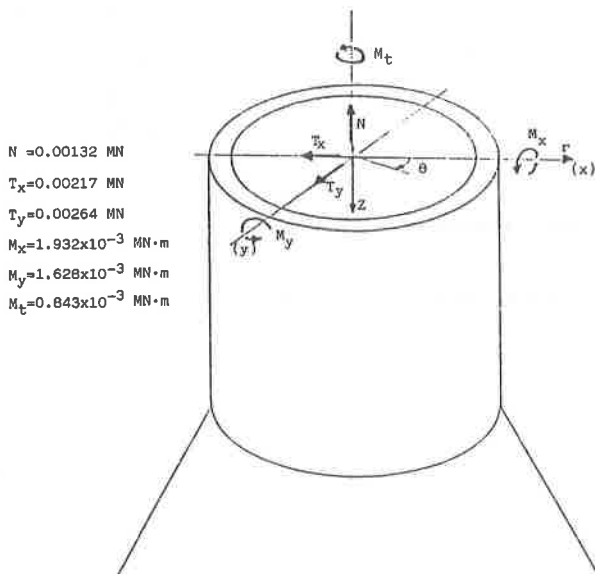


Fig.6 - Primary charges on the nozzle terminal section

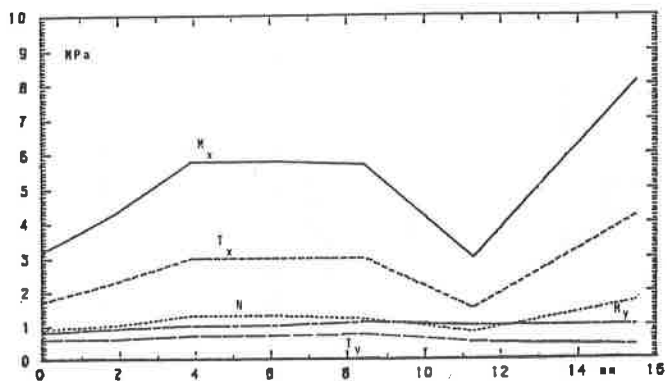


Fig.7a - Equivalent stress distribution on section B for each primary charge component

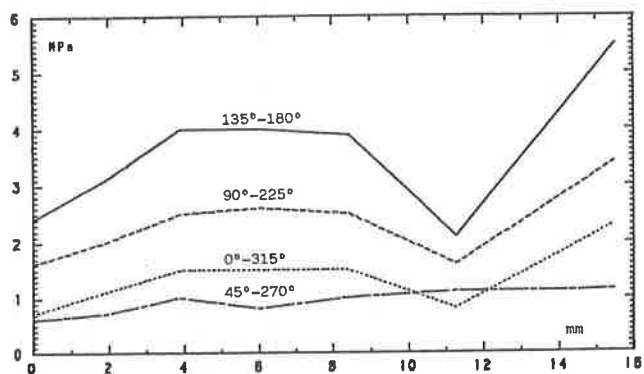


Fig.7b - Resultant equivalent stress distribution on section B

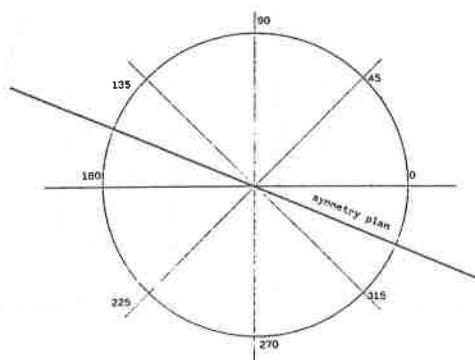


Fig.8 - Critical symmetric plane

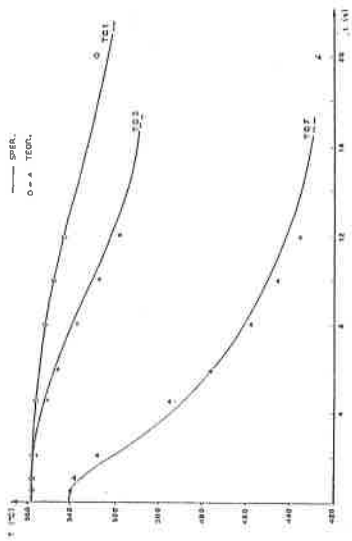


Fig. 9 - Theoretical-experimental comparison of temperature trend

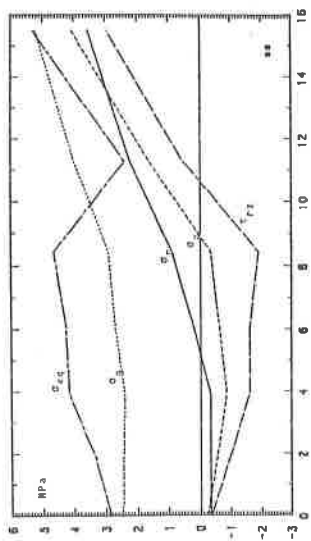


Fig. 11 - Equivalent stress and single component due to an 'equivalent' traction change in section B

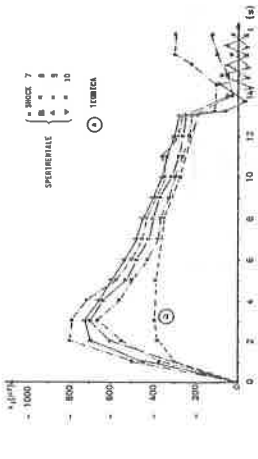


Fig. 10a - Theoretical-experimental comparison of the axial strain

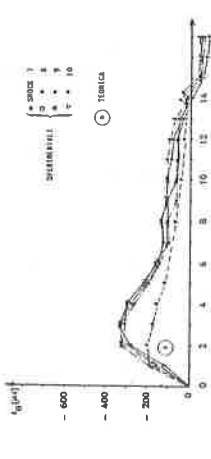


Fig. 10b - Theoretical-experimental comparison of the hoop strain

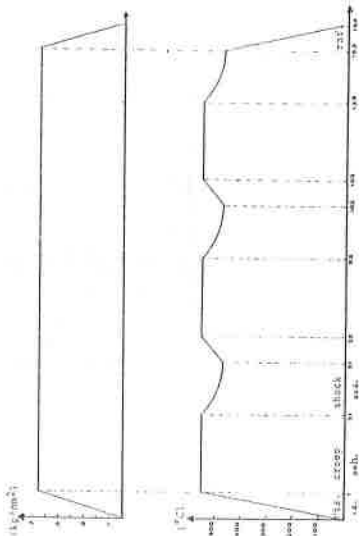


Fig. 12 - Thermal and mechanical charges for inelastic analysis